



HAL
open science

Generating liquid nanojets from copper by dual laser irradiation for ultra-high resolution printing

Qingfeng Li, A.P. Alloncle, David Grojo, P. Delaporte

► **To cite this version:**

Qingfeng Li, A.P. Alloncle, David Grojo, P. Delaporte. Generating liquid nanojets from copper by dual laser irradiation for ultra-high resolution printing. *Optics Express*, 2017, 25 (20), pp.24164. 10.1364/OE.25.024164 . hal-02138435

HAL Id: hal-02138435

<https://hal.science/hal-02138435>

Submitted on 23 May 2019

HAL is a multi-disciplinary open access archive for the deposit and dissemination of scientific research documents, whether they are published or not. The documents may come from teaching and research institutions in France or abroad, or from public or private research centers.

L'archive ouverte pluridisciplinaire **HAL**, est destinée au dépôt et à la diffusion de documents scientifiques de niveau recherche, publiés ou non, émanant des établissements d'enseignement et de recherche français ou étrangers, des laboratoires publics ou privés.



Generating liquid nanojets from copper by dual laser irradiation for ultra-high resolution printing

QINGFENG LI,* ANNE PATRICIA ALLONCLE, DAVID GROJO, AND PHILIPPE DELAPORTE

Aix-Marseille University, CNRS, LP3, F-13288 Marseille, France

*li@lp3.univ-mrs.fr

Abstract: When the energy of a short laser pulse is localized in a fluid material, a flow motion is induced that can lead to the generation of free-surface jets. This nozzle-free jetting process is exploited to print conductive materials, typically metal nanoparticle inks, but this approach remains limited to the transfer of low viscosity fluids with a minimum feature size of few micrometers. We introduce a dual-laser method to achieve reproducible high-aspect-ratio jets from thin solid films. A first laser irradiation induces the melting of copper thin films and a second synchronized short pulse irradiation initiates the jetting process. Using time-resolved microscopy, we investigate the influence of the film thickness on the flow motion mechanisms and the ejection dynamics. For a wide range of laser fluences, we present observations similar to those obtained when the jets are generated by a single laser pulse from liquid donor films. The use of a solid film allows reducing the film thickness and then the volume of transferred material. Finally, we analyze these results in the perspective of using this double pulse LIFT technique for additive manufacturing of nano-micro-structures. Stable jets are formed from the copper films over distances exceeding 50- μm and are exploited to demonstrate periodic printing of 1.5- μm diameter droplets.

© 2017 Optical Society of America

OCIS codes: (140.3390) Laser materials processing; (220.4610) Optical fabrication; (100.0118) Imaging ultrafast phenomena; (310.0310) Thin films; (160.3900)Metals; (160.4236) Nanomaterials.

References and links

1. W. S. Rayleigh, "On the stability of jets," *Proc. Lond. Math. Soc.* **4**, 10–13 (1878).
2. Y. Wang, X. Liu, K.-S. Im, W.-K. Lee, J. Wang, K. Fezzaa, D. L. S. Hung, and J. R. Winkelman, "Ultrafast X-ray study of dense-liquid-jet flow dynamics using structure-tracking velocimetry," *Nat. Phys.* **4**(4), 305–309 (2008).
3. J. Bohandy, B. F. Kim, and F. J. Adrian, "Metal deposition from a supported metal film using an excimer laser," *J. Appl. Phys.* **60**(4), 1538–1539 (1986).
4. P. Delaporte and A.-P. Alloncle, "Laser-induced forward transfer: A high resolution additive manufacturing technology," *Optics & Laser Technology* **78**, 33–41 (2016).
5. L. Rapp, A. K. Diallo, A. P. Alloncle, C. Vidélot-Ackermann, F. Fages, and P. Delaporte, "Pulsed-laser printing of organic thin-film transistors," *Appl. Phys. Lett.* **95**(17), 1–4 (2009).
6. M. Makrygianni, E. Verrelli, N. Boukos, S. Chatzandroulis, D. Tsoukalas, and I. Zergioti, "Laser printing and characterization of semiconducting polymers for organic electronics," *Appl. Phys., A Mater. Sci. Process.* **110**(3), 559–563 (2013).
7. R. Fardel, M. Nagel, F. Nüesch, T. Lippert, and A. Wokaun, "Fabrication of organic light-emitting diode pixels by laser-assisted forward transfer," *Appl. Phys. Lett.* **91**(6), 061103 (2007).
8. N. T. Kattamis, N. D. McDaniel, S. Bernhard, and C. B. Arnold, "Ambient laser direct-write printing of a patterned organo-metallic electroluminescent device," *Org. Electron.* **12**(7), 1152–1158 (2011).
9. F. Di Pietrantonio, M. Benetti, D. Cannatà, E. Verona, A. Palla-Papavlu, V. Dinca, M. Dinescu, T. Mattle, and T. Lippert, "Volatile toxic compound detection by surface acoustic wave sensor array coated with chemoselective polymers deposited by laser induced forward transfer: Application to sarin," *Sens. Actuators B Chem.* **174**, 158–167 (2012).
10. C. Boutoupoulos, E. Touloupakis, I. Pezzotti, M. T. Giardi, and I. Zergioti, "Direct laser immobilization of photosynthetic material on screen printed electrodes for amperometric biosensor," *Appl. Phys. Lett.* **98**(9), 093703 (2011).
11. A. J. Birnbaum, K. Heungsoo, N. A. Charipar, and A. Piqué, "Laser printing of multi-layered polymer/metal heterostructures for electronic and MEMS devices," *Appl. Phys., A Mater. Sci. Process.* **99**(4), 711–716 (2010).

12. L. Koch, A. Deiwick, S. Schlie, S. Michael, M. Gruene, V. Coger, D. Zychlinski, A. Schambach, K. Reimers, P. M. Vogt, and B. N. Chichkov, "Skin tissue generation by laser cell printing," *Biotechnol. Bioeng.* **109**(7), 1855–1863 (2012).
13. S. Catros, J.-C. Fricain, B. Guillotin, B. Pippenger, R. Bareille, M. Remy, E. Lebraud, B. Desbat, J. Amédée, and F. Guillemot, "Laser-assisted bioprinting for creating on-demand patterns of human osteoprogenitor cells and nano-hydroxyapatite," *Biofabrication* **3**(2), 025001 (2011).
14. C. L. Sones, M. Feinaeugle, A. Sposito, B. Gholipour, and R. W. Eason, "Laser-Induced Forward Transfer-printing of focused ion beam pre-machined crystalline magneto-optic yttrium iron garnet micro-discs," *Opt. Express* **20**(14), 15171–15179 (2012).
15. C. Florian, S. Piazza, A. Diaspro, P. Serra, and M. Duocastella, "Direct Laser Printing of Tailored Polymeric Microlenses," *ACS Appl. Mater. Interfaces* **8**(27), 17028–17032 (2016).
16. M. Duocastella, J. M. Fernández-Pradas, J. L. Morenza, and P. Serra, "Time-resolved imaging of the laser forward transfer of liquids," *J. Appl. Phys.* **106**(8), 084907 (2009).
17. A. Pique, R. C. Y. Auyeung, H. Kim, K. M. Metkus, and S. A. Mathews, "Digital microfabrication by laser decal transfer," *J. Laser Micro/Nanoeng.* **3**(3), 163–169 (2008).
18. D. P. Banks, C. Grivas, J. D. Mills, R. W. Eason, and I. Zergioti, "Nanodroplets deposited in microarrays by femtosecond Ti:sapphire laser-induced forward transfer," *Appl. Phys. Lett.* **89**(19), 87–90 (2006).
19. J. A. Grant-Jacob, B. Mills, M. Feinaeugle, C. L. Sones, G. Oosterhuis, M. B. Hoppenbrouwers, and R. W. Eason, "Micron-scale copper wires printed using femtosecond laser-induced forward transfer with automated donor replenishment," *Opt. Mater. Express* **3**(6), 747–754 (2013).
20. A. I. Kuznetsov, R. Kiyam, and B. N. Chichkov, "Laser fabrication of 2D and 3D metal nanoparticle structures and arrays," *Opt. Express* **18**(20), 21198–21203 (2010).
21. C. W. Visser, R. Pohl, C. Sun, G.-W. Römer, B. Huis in 't Veld, and D. Lohse, "Toward 3D Printing of Pure Metals by Laser-Induced Forward Transfer," *Adv. Mater.* **27**(27), 4087–4092 (2015).
22. M. Zenou and Z. Kotler, "Printing of metallic 3D micro-objects by laser induced forward transfer," *Opt. Express* **24**(2), 1431–1446 (2016).
23. A. Narazaki, Y. Kurosaki, T. Sato, Y. Kawaguchi, and H. Niino, "On-demand deposition of functional oxide microdots by double-pulse laser-induced dot transfer," *J. Laser Micro/Nanoeng.* **9**(1), 10–14 (2014).
24. A. Klini, P. A. Loukakos, D. Gray, A. Manousaki, and C. Fotakis, "Laser induced forward transfer of metals by temporally shaped femtosecond laser pulses," *Opt. Express* **16**(15), 11300–11309 (2008).
25. C. Boutopoulos, I. Kalpyris, E. Serpetzoglou, and I. Zergioti, "Laser-induced forward transfer of silver nanoparticle ink: Time-resolved imaging of the jetting dynamics and correlation with the printing quality," *Microfluid. Nanofluid.* **16**(3), 493–500 (2014).
26. R. Pohl, C. W. Visser, G.-W. Römer, D. Lohse, C. Sun, and B. Huis in 't Veld, "Ejection regimes in picosecond laser-induced forward transfer of Metals," *Phys. Rev. Applied* **3**(2), 024001 (2015).
27. B. N. Chichkov, C. Momma, S. Nolte, F. von Alvensleben, and A. Tünnermann, "Femtosecond, picosecond and nanosecond laser ablation of solids," *Appl. Phys., A Mater. Sci. Process.* **63**(2), 109–115 (1996).
28. A. I. Kuznetsov, C. Unger, J. Koch, and B. N. Chichkov, "Laser-induced jet formation and droplet ejection from thin metal films," *Appl. Phys., A Mater. Sci. Process.* **106**(3), 479–487 (2012).
29. M. Zenou, A. Sa'ar, and Z. Kotler, "Laser jetting of femto-liter metal droplets for high resolution 3D printed structures," *Sci. Rep.* **5**, 17265 (2015).
30. N. Chigier and R. D. Reitz, *Recent Advances in Spray Combustion: Spray Atomization Drop Burning Phenomena* (AIAA, 1996), Chap. Regimes of jet breakup and breakup mechanisms (Physical Aspects), 109–135.
31. E. Biver, L. Rapp, A. P. Alloncle, and P. Delaporte, "Multi-jets formation using laser forward transfer," *Appl. Surf. Sci.* **302**, 153–158 (2014).
32. L. Battezzati and A. L. Greer, "The viscosity of liquid metals and alloys," *Acta Metall.* **37**(7), 1791–1802 (1989).
33. C. Unger, J. Koch, L. Overmeyer, and B. N. Chichkov, "Time-resolved studies of femtosecond-laser induced melt dynamics," *Opt. Express* **20**(22), 24864–24872 (2012).
34. M. S. Brown, C. F. Brasz, Y. Ventikos, and C. B. Arnold, "Impulsively actuated jets from thin liquid films for high-resolution printing applications," *J. Fluid Mech.* **709**, 341–370 (2012).
35. U. Zywiets, A. B. Evlyukhin, C. Reinhardt, and B. N. Chichkov, "Laser printing of silicon nanoparticles with resonant optical electric and magnetic responses," *Nat. Commun.* **5**, 3402 (2014).

1. introduction

Liquid jet formation is a basic phenomenon which has been extensively studied for more than a century because of its importance in various natural processes and applications [1, 2]. Its occurrence relies on multiple interactions between complex hydrodynamic mechanisms and on many material properties, including surface tension and viscosity. Nozzle-based ink-jet printing is one of the examples of an industrial printing process developed thanks to the control of the dynamics of such liquid jets. However, the next engineering challenge is to achieve submicrometer

resolution printing of any material for advanced 3D additive nano- micro-fabrication.

Laser-induced forward transfer (LIFT) [3] whose basic concept consists in the backside laser irradiation of a thin donor film to transfer small amounts of material on a target set nearby has already shown its potential for printing applications [4] in microelectronics [5, 6], OLEDs [7, 8], sensors [9, 10], MEMS [11], biomedical engineering [12, 13] and micro-optical elements [14, 15]. The method can be applied to fluids including liquids, inks [16] or pastes [17] providing intrinsically improved printing resolution compared to nozzle-based techniques because micro-jetting is achieved from thin donor films (1-100 μm). Another unique advantage of LIFT is the possibility to transfer materials in solid phase. This process is driven by laser-induced mechanical breakup of the thin donor film and the ejection of solid pixels with minimum feature sizes down to $\approx 10 \mu\text{m}$.

A potential solution for a versatile ultra-high resolution printing solution was revealed when an ultrashort laser pulse was used to create a liquid jet from a solid material [18]. However, the approach has not been so far widely adopted due to its practical complexity [19–22]. This arises because one needs to achieve with a single laser interaction unlikely conditions to first melt the solid material and control the balance between surface tension and viscosity, and second to provide the right amount of energy to induce the appropriate fluid motion for the formation of free-surface liquid jets. In practice, this leads to extremely narrow and material-specific processing windows (when existing).

Here, we introduce a double-pulse concept to address these limitations linked to the transfer in liquid phase from a solid film. Laser printing with a double-pulse approach has previously been reported using trains of identical pulses either in the nanosecond [23] or femtosecond [24] regime. These studies showed some improvements of the printing performances but without investigation of the transfer mechanisms behind these observations. Our approach is based on the use of two laser pulses, with different pulse duration, and an accurate control of each pulse energy and of the delay between them. The motivation is to independently control change of the material properties thanks to the first microsecond pulse and to induce the material ejection with the second ultrashort laser pulse. We use time-resolved microscopy to study the laser induced formation and propagation of high-velocity nanojets from solid copper films. When uniform local melting of the film is achieved, the second laser pulse leads to the generation of long and stable jets, similar to those generated from inks by single laser irradiation [25], for an impressively large range of laser parameters. Finally we print a matrix of micrometer copper dots with the double-pulse LIFT approach to demonstrate its potential for the challenging additive fabrication of microdevices or architected multi-materials.

2. Methods

2.1. Single- and double-pulse LIFT

Our experimental arrangement is depicted in Fig. 1(a). It allows performing: single or double-pulse LIFT, time-resolved shadowgraphy of material transfer (lateral imaging) and precise positioning of laser beams and materials. The laser source used to achieve the melting of the donor film is a so-called quasi-continuous wave (QCW) laser (IPG Photonics, YLR-150/1500-QCW-AC-Y14) emitting, at 1070-nm wavelength, pulses of variable duration from 50 μs to the continuous wave operation. After this first QCW laser irradiation, a Nd:YAG picosecond laser (Continuum, Leopard S10/20) delivers, at 355-nm wavelength (third harmonic), pulses of 50-ps duration (FWHM) which are focused at the center of the melted region to induce material ejections. To do so, both beams enter collinearly through the same microscope objective (Olympus, Plan Achromat, NA=0.40). The spot diameter at the copper-donor interface with the picosecond laser is expected to be $\approx 1 \mu\text{m}$. To achieve a much larger melted area, the spot size of the QCW laser is increased by focusing the beam before the objective using a lens. According to the observation of the modified regions, the spot diameter is about 130 μm at the copper film

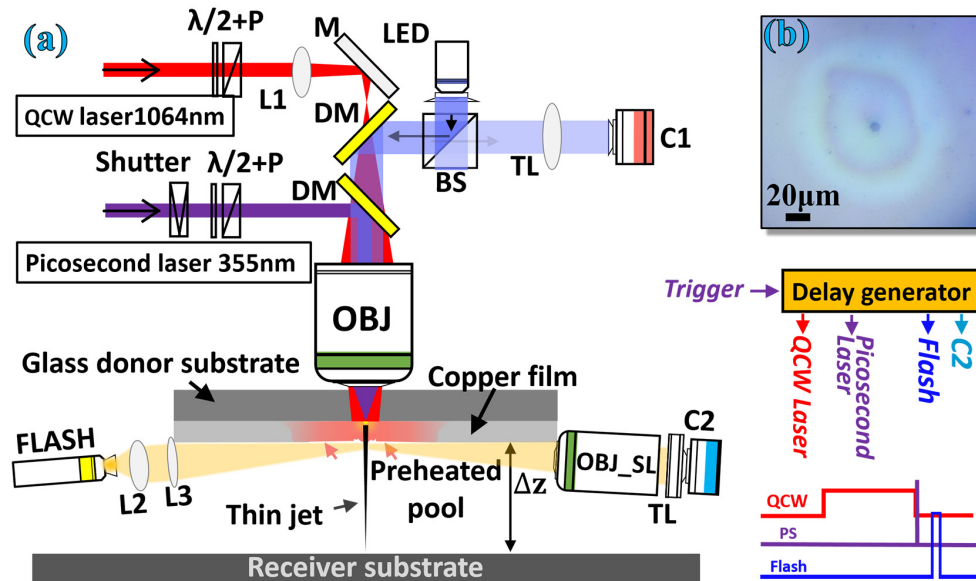


Fig. 1. (a) Experimental arrangement. Beam paths of the pre-heating (QCW) and the picosecond lasers are displayed in red and purple respectively. $\lambda/2$, half-wave plate; P, polarizer; BS, beam splitter; TL, tube lens; OBJ, objective lens; FLASH, nanosecond flash lamp; OBJ_SL, super-long working distance objective lens; C1 and C2, cameras; L1, L2 and L3, lenses; DM, dichroic mirror; M, mirror. (b) Optical image of a modified region of a copper donor film after double-pulse processing. The timing sequence of our experiment has been set as that the picosecond pulse is synchronized with respect to the falling edge of the sub-millisecond pulse and the flash illuminate the ejections with a tunable delay.

surface. The power of both lasers are independently adjusted using half-wave plate and polarizer combinations. The positioning of the two beams and the systematic inspection of the donor film is facilitated by a customized reflection microscopy arrangement. As an illustration, an image of the donor copper film after a double-pulse irradiation is shown in Fig. 1(b). On this image, one can see a central small dark spot corresponding to the residual crater left after the material ejection and a surrounding bright circular region corresponding to the zone pre-melted by the QCW laser pulse.

2.2. Time-resolved observation of the ejections

Time-resolved shadowgraphs of material ejections are recorded using a CCD camera (QImaging, QICAM) mounted on a second customized microcopy arrangement based on a long working distance microscope objective (Mitutoyo, M Plan Apo SL, NA=0.28) and a tube lens for 20 \times magnification. Bright-field flash illumination is provided by a NANOLITE nanosecond flash lamp (High-Speed Photo-Systeme, KL-M). The flash duration of 12 ns determines the temporal resolution of the acquisition system. A digital delay generator (Stanford Research Systems, DG645) is used to precisely synchronize, with adjustable delay, the double-pulse process with shadowgraph imaging. As shown with the inserted chronogram in Fig. 1 (bottom right), we set the double-pulse sequence by precise synchronization of the picosecond pulse with respect to the falling edge of the sub-millisecond pulse.

3. Results and discussion

3.1. Single- and double-pulse LIFT with different donor thicknesses

Donor copper films with thicknesses from 180 nm to 620 nm are deposited on glass microscope slides by thermal evaporation. Figure 2 presents shadowgraphy images of material ejections from those films obtained for both single-pulse and double-pulse LIFT experiments while the laser fluence is varied. To compare the typical features in each situation, the delay for shadowgraph imaging has been adjusted in the range 250-300 ns depending on conditions. Figures 2(a1)-2(a3) show ejections from a 180 nm copper film induced by a single picosecond pulse irradiation. Ejections under similar situations have already been observed and explained [26]: for low and intermediate fluence regimes ($F \leq 720 \text{ mJ/cm}^2$), cap-like and elongated features (also called jet-like) are observed, and for the high fluence regime ($F \geq 1000 \text{ mJ/cm}^2$), uncontrollable spraying processes occur. The physical mechanisms corresponding to each regime are thermally-induced stress for the cap-like regime, fluid motion of the melted layer for the jet-like regime and partial evaporation for the spraying regime [26]. For comparison, Figs. 2(a4)-2(a6) show ejections by double-pulse LIFT corresponding to conditions similar to the single-pulse ejections except that a first-pulse of 120- μs duration and 2.57-mJ energy (QCW laser) is applied to melt the film before the material ejection. We can observe that the ejection dynamics are very similar to those generated by a single laser pulse, whatever the fluence. To explain that, we must consider the thermally affected depth $l_{th} = 2\sqrt{D\tau}$ (D : thermal diffusion coefficient, τ : pulse duration) [27], induced by the picosecond pulse irradiation which is about 150 nm. This value being very close to the thickness of the copper film, there is only a modest temperature gradient created throughout the whole film thickness, while a strong gradient is required for the generation of stable liquid jets.

In order to achieve stronger temperature gradients in such a thin film and demonstrate the potential of the double pulse LIFT approach, one option would be to use shorter pulses, down to femtosecond regime, to reduce the thermally affected depth. However, for simplicity reasons, we chose to use thicker films while keeping the same irradiation conditions. First, we have repeated the experiments with a 410-nm thick copper donor film. For the double-pulse LIFT ejections shown in Figs. 2(b4)-2(b6), the formation of stable, uniform and long jets is observed over a range of laser fluences from 530 to 1000 mJ/cm^2 . The afterward re-solidified jet at the donor substrate surface observed in these conditions, shown in Fig. 2(d2), points out the motion of the melted copper at the donor free surface. This image confirms that the ejection mechanism is based on a fluid mechanic process [28]. All images of ejection have been captured at the same time delay of 280-ns, thus the difference of lengths is related to the increasing jet propagation velocities with the deposited energy. For single-pulse LIFT [see Figs. 2(b1)-2(b3)], we observe when increasing the fluence, a significant elongation of the jet-like behavior. In this configuration, the copper film thickness (410 nm) is 2.5 times thicker than the thermally affected depth within the picosecond pulse duration. Then, a laser fluence value can be found for inducing the melting of the whole layer together with the vaporization of a suitable amount of copper at the interface with the glass substrate to induce enough force for fluid motion and jet formation. As suggested by M. Zenou *et al.* [29], when the melted material front reached the free surface there exist some solid barriers around the central melted region leading to a so-called thermally induced nozzle (TIN) transfer. Figure 2(d1) shows such a quasi-nozzle at the donor surface that illustrates this process. It is worth noting that even if we qualify the process as jet transfer because of the elongated shape of the material seen in the shadowgraphy images, the jets are not as uniform and well-defined as those of the double-pulse LIFT [see Figs. 2(b4)-2(b6)] highlighting the differences of mechanisms occurring in single and double-pulse LIFT.

For further investigation and to enhance these differences, we also used a 620-nm thick copper film as donor. With single-pulse LIFT, when the fluence is lower than 2410 mJ/cm^2 [refers to

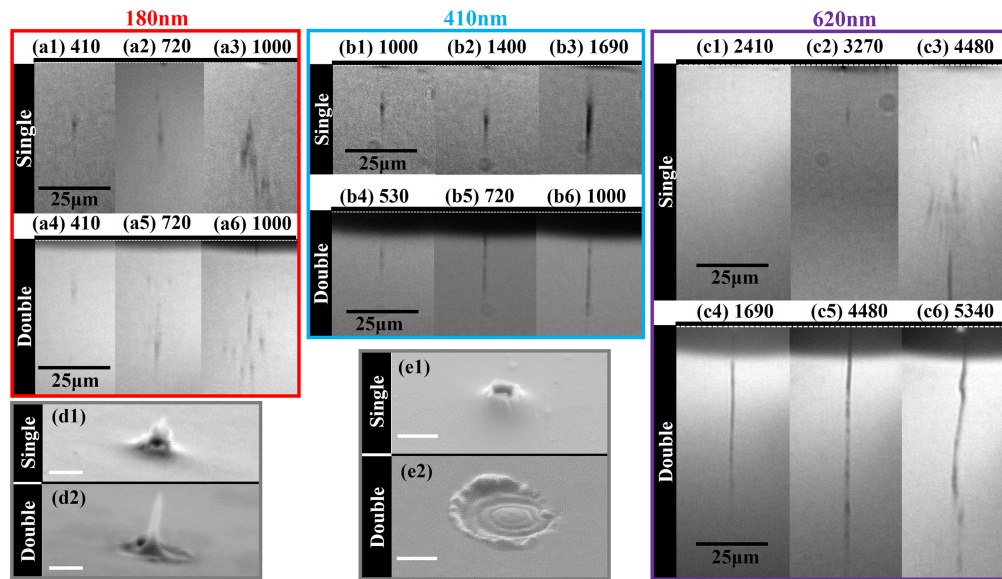


Fig. 2. Shadowgraph imaging of the ejection from copper films of different thicknesses: (a) 180-nm, (b) 410-nm, (c) 620-nm. (a1-a3), (b1-b3) and (c1-c3) are ejections induced by single picosecond pulses with different fluences given at the top of each image (unit: mJ/cm^2). (a4-a6), (b4-b6) and (c4-c6) are ejections induced by double-pulse LIFT with different picosecond pulse fluences given at the top of each image (unit: mJ/cm^2) and a first pre-melting pulse with respective duration and energy of $120 \mu\text{s}$ and 2.6 mJ for 180-nm films, $200 \mu\text{s}$ and 4.3 mJ for 410-nm films and $250 \mu\text{s}$ and 13.4 mJ for 620-nm films. (d1) and (d2) are SEM images of the residual crater left on the 410-nm donor film after single (b1) and double (b6) pulse LIFT (scale bars: $1 \mu\text{m}$). (e1) and (e2) are residual craters left on the 620-nm donor film after single (c2) and double (c5) pulse LIFT (scale bars: $2 \mu\text{m}$). For each ejection image, the white dash line stands for the location of the donor film and the shady region near the donor film is due to tilted imaging and laser-induced changes of the surface reflectivity.

Fig. 2(c1)], the copper film is not fully melted or evaporated and the deformation force generated in the confined interaction volume is not strong enough to induce any material transfer. For a medium fluence such as $3270 \text{ mJ}/\text{cm}^2$ [refers to Fig. 2(c2)], a TIN transfer is obtained. The corresponding quasi-nozzle on the donor film is shown in Fig. 2(e1). For higher fluences such as $4400 \text{ mJ}/\text{cm}^2$ [refers to Fig. 2(c3)] the free surface is melted leading to the formation of a well-defined liquid jet (partially visible at the bottom of the image), but a larger amount of copper is vaporized inducing also a spray-like ejection behind the jet. In these cases, the deposition becomes very hardly controllable and debris are systematically found on the receiver substrate after transfer (not shown here). By contrast, for double-pulse LIFT ejections shown in Figs. 2(c4)-2(c6), the energy of the picosecond laser pulse is systematically deposited in a fully melted liquid layer thanks to the irradiation with the QCW laser pre-pulse. This makes possible the formation of stable, uniform and long jets over a large range of fluences. They are observed along distances exceeding $60 \mu\text{m}$ and the fluence process window for jet formation with the picosecond laser ranges from $1690 \text{ mJ}/\text{cm}^2$ to $4480 \text{ mJ}/\text{cm}^2$. Moreover, Fig. 2(e2) presents a SEM image of re-solidified copper on the donor surface after such double-pulse LIFT. In this thick copper film case, the observed ripples are due to fluid motion in the melted copper pool and revealed here by the fast re-solidification process.

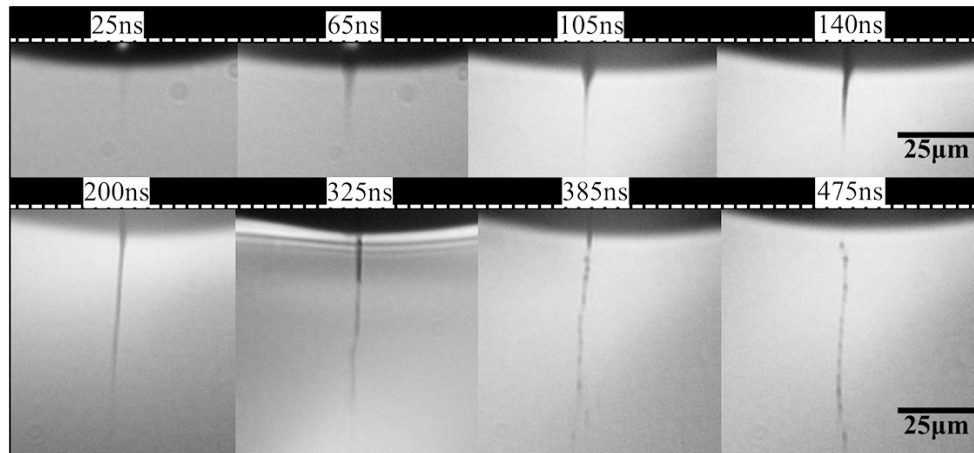


Fig. 3. Time-resolved shadowgraphy images acquired for double-pulse LIFT with a 620-nm copper film.

3.2. Time-resolved shadowgraphs of double-pulse induced jets

For further investigation of these jetting behaviors, time-resolved shadowgraphs of double-pulse LIFT from a 620-nm copper film are shown in figure 3. As for figures 2(c4)-2(c6), a first-pulse with 250- μ s duration and 13.4-mJ energy pre-melts the copper film and a picosecond pulse with 3620-mJ/cm² fluence induces the transfer that is imaged for different delays from 25 to 475 ns. As previously observed [25], the transfer process starts with the surface deformation, that can be attributed to the generation of a localized vapor due to the evaporation of the copper at the film-substrate interface, inducing the fluid motion and the jet formation. This deformation has a triangular shape and can be observed until a delay of about 150 ns. Then, the jet progressively elongates reaching its longest and most uniform morphology at 200 ns. Eventually, for delays exceeding 325 ns, the jet detaches from the donor surface and further breaks up into droplets due the Rayleigh-Plateau instability [30]. Therefore, when the gap between donor and receiver is large ($> 50 \mu\text{m}$ in here discussed situation), this instability may result in pieces of the jet that break off and are deposited as satellite droplets on the receiver. This dynamics of the jet formation and expansion is similar to the one observed for the LIFT of silver nanoparticle inks in the picosecond regime [31]. Interestingly, melted copper and silver inks exhibit both a viscosity of few millipascal-seconds [32] making reasonable the hypothesis of identical fluid motion mechanisms. It is worth noting that the fluences required to initiate these jets are more than one order of magnitude higher for melted copper than for silver inks. That is due to first the low evaporation temperature of ink solvents compared to bulk copper and second the higher material density of copper compared to silver inks containing only 20% of metal.

3.3. Discussion

When a single 50 ps picosecond laser beam irradiates the thick solid metal film through the glass substrate, the temperature gradient induced in the metal can lead to the formation of three phases: a solid layer near the metal air interface, a "vaporized material" layer near the donor-substrate interface and a liquid layer between the two previous ones. The thickness of each layer depends on the laser fluence and the time delay after the irradiation. The importance of these layers has been discussed in [26]. The pressure increase in the volume of vaporized layer will provide the kinetic energy required to induce the fluid motion, and eventually to break the solid layer in order to form a thermally induced nozzle (TIN) as suggested in [29]. As a first

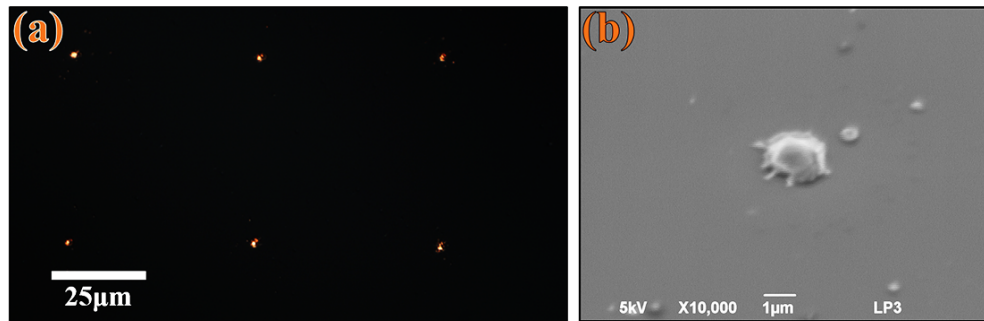


Fig. 4. (a) Array of copper droplets printed by double-pulse LIFT from a 410-nm donor film. (b) SEM image of a single copper droplet of this array.

conclusion, our observations suggest two critical prerequisites for the formation of liquid copper jets: first, the donor film must be melted over its full thickness; second, the local temperature and pressure conditions at the substrate-donor film interface must be high enough to induce a partial vaporization of the film and generate a sufficient deformation force. These criteria are obviously difficult to fulfill together with a single pulse irradiation and, when successful, lead to very narrow and material-specific processing windows [33]. Interestingly, we show that the use of a QCW laser allows to locally rise uniformly the temperature of the film, and ultimately its melting over its full thickness. Then, the subsequent irradiation with a short laser pulse brings the appropriate amount of energy required to induce the jetting mechanisms. This dual-laser method provides the freedom to accurately control the film properties and the material transfer independently. In double pulse LIFT mode, the picosecond laser irradiates a pre-melted liquid layer, and its unique purpose is to vaporize a sufficient volume of the layer near the substrate-donor interface in order to rise the pressure in this confined volume and provide the kinetic energy required to induce the fluid motion. In this configuration, the jet formation relies on the volume expansion of the vaporized metal and the mechanisms are similar to those described for the blister LIFT [34].

Finally, to demonstrate the potential of this double-pulse approach for the printing in liquid phase of initially solid materials, we have set a silicon receiver substrate at $\approx 55 \mu\text{m}$ in front of the donor substrate and used the same conditions as those described in figure 2(b6) to form a uniform thin jet. In this experiment, we repeated the double-pulse LIFT at different locations of the receiver surface separated by $50 \mu\text{m}$ to print a regular array of copper droplets. Figure 4(a) presents an optical image of a region of the printed array. Because of the small size of the droplets, near the resolution limit for wide field microscopy, we have used dark-field microscopy for contrasted imaging of the feature locations. Figure 4(b) is a SEM image of a typical solidified copper droplet printed on the receiver. Each droplet exhibits a diameter of around $1.5 \mu\text{m}$. The process being not fully optimized, we can observe few nano-droplets next to the main one. They are due to the breaking of the thin copper jet before reaching the surface. However, the transfer of the melted metal in jet ejection regime avoids the generation of debris generally observed with single pulse LIFT in cap or spray ejection regime [21, 26]. The generation of long and stable liquid metal jets thanks to the double pulse LIFT approach will help the printing of debris-free structures.

These results also point out the current limitation of the setup to address the challenge of nano-printing. The transfer of sub-micrometer pixels requires the use of a thinner metal film. In such conditions the generation of a temperature gradient to vaporize only a small layer of the film make the use of an ultrashort pulse, in the femtosecond regime, necessary.

4. Conclusions

In conclusion, we have reported the formation and expansion of liquid metal jets from a solid metal film thanks to a double-pulse irradiation process. Long and stable liquid metal jets have been observed for a wide range of irradiation conditions and film thicknesses. We have concentrated the demonstration on copper but the concept is general and can be directly applied to any pure metals, alloys, and semiconductors. Provided that ultrashort pulses are used, the approach is also likely compatible with material transfer from ultra-thin films which is a challenging requirement for the consistent printing of nanodots [35]. This must open a way for the flexible synthesis of 3D microstructures (e.g. bio-inspired architectures) and ultimately advanced nanomaterials as metasurfaces and 3D photonic crystals which are today inaccessible by LIFT.